Chapter 10

MULTILINEAR INTERVAL SYSTEMS: THE MAPPING THEOREM

In this chapter we deal with robust stability problems where the uncertain interval parameters appear *multilinearly* in the characteristic polynomial coefficients. We introduce the Mapping Theorem which reveals a fundamental property of the image set of such systems. This property allows us to effectively approximate the image set evaluated at an arbitrary point in the complex plane by overbounding it with a union of convex polygons; moreover the accuracy of this approximation can be increased as much as desired. A computationally efficient solution to the robust stability problem can then be obtained by replacing the multilinear interval family with a test set consisting of a polytopic family. We also show how various worst case stability and performance margins over the interval parameter set can be estimated from this polytopic test set. These include gain and phase margins, H_∞ norms, absolute stability under sector bounded nonlinear feedback, and guaranteed time-delay tolerance.

10.1 INTRODUCTION

We begin by giving some examples of system models where parameters appear naturally in a multilinear form. A function $f(x_1, x_2, \cdots, x_n)$ is *multilinear* (*multiaffine*) if for each $i \in [1, 2, \cdots, n]$, f is a linear (affine) function of x_i when the $x_j, j \neq i$ are held constant. We shall use the term multilinear loosely to include the multiaffine case.

Multiloop Systems

Consider the signal flow graph of a multiloop system as shown in Figure 10.1.

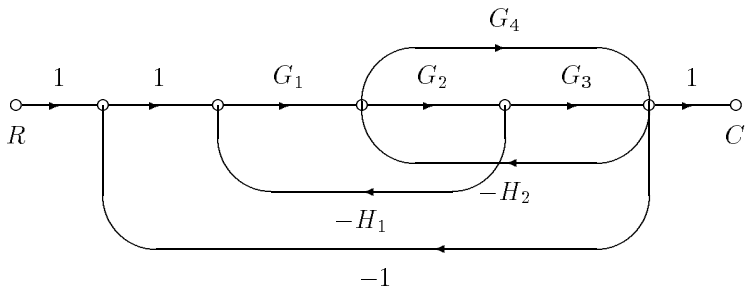

Figure 10.1. Signal flow graph

The closed loop transfer function is

$$\frac{C(s)}{R(s)} = \frac{G_1G_2G_3 + G_1G_4}{1 + G_1G_2H_1 + G_2G_3H_2 + G_1G_2G_3 + G_4H_2 + G_1G_4}.$$

We see that the numerator and denominator of the transfer function is a multilinear function of the gains G_i and H_j of the branches. If these transfer functions contain a vector of parameters appearing linearly in their coefficients then the closed loop transfer function coefficients will be multilinear functions of these parameters. This situation is, of course, not peculiar to this example and it is true that multilinear dependence holds generically in signal flow graphs.

State Space Models

Consider the state space equations of a system

$$\dot{x} = Ax + Bu.$$

The characteristic polynomial of the system, which determines whether it is stable or not is

$$\delta(s) = \det\left[sI - A\right].$$

It can be easily seen that the coefficients of the characteristic polynomial are multilinear functions of the entries a_{ij} of the matrix A. State space equations are frequently written with the states denoting physical variables such as currents, voltages, positions and velocities. It will therefore often be the case that distinct elements of the matrix A represent independent physical parameters. More generally, if uncertain parameters appear in multiple locations in the matrix A but have a "rank-one" structure the characteristic polynomial will once again be a multilinear function of these parameters.

Matrix Fraction Description with Interval Elements

Suppose that $G(s) = N(s)D^{-1}(s)$ and $C(s) = D_c^{-1}(s)N_c(s)$ represent matrix fraction descriptions of a plant and controller connected in a feedback loop. The characteristic polynomial of the closed loop system is

$$\delta(s) = \det\left[D_c(s)D(s) + N_c(s)N(s)\right]$$

If $C(s)$ is fixed and $G(s)$ contains parameter uncertainty it may be reasonable to model this by allowing the elements of $D(s)$ and $N(s)$ to be independent interval uncertain polynomials. It is now straightforward to verify that $\delta(s)$ is a multilinear function of the polynomials in $D(s)$ and $N(s)$ and consequently a multilinear function of the interval coefficients.

The point of the above examples is to show that multilinear parameter dependencies occur in a wide variety of system models. This is fortunate for us. Even though robustness issues in the general nonlinear dependency case are quite difficult to handle, efficient techniques are available for multilinear systems. A key result is the Mapping Theorem which will allow us to determine robust stability in a computationally effective manner. It will also allow us to determine various worst case stability margins and performance measures (robust performance) in the presence of parameter uncertainty.

10.2 THE MAPPING THEOREM

The Mapping Theorem deals with a family of polynomials which depend multilinearly on a set of interval parameters. We refer to such a family as a Multilinear Interval Polynomial. The Mapping Theorem shows us that the image set of such a family is *contained* in the convex hull of the image of the vertices. We state and prove this below.

Let $\mathbf{p} = [p_1, p_2, \cdots, p_l]$ denote a vector of real parameters. Consider the polynomial

$$\delta(s, \mathbf{p}) := \delta_0(\mathbf{p}) + \delta_1(\mathbf{p})s + \delta_2(\mathbf{p})s^2 + \cdots + \delta_n(\mathbf{p})s^n \tag{10.1}$$

where the coefficients $\delta_i(\mathbf{p})$ are *multilinear* functions of $\mathbf{p}$, $i = 0, 1, \cdots n$. The vector $\mathbf{p}$ lies in an uncertainty set

$$\mathbf{\Pi} := \left\{\mathbf{p} \ : \ p_i^- \le p_i \le p_i^+, \quad i = 1, 2, \cdots, l\right\}. \tag{10.2}$$

The corresponding set of *multilinear interval polynomials* is denoted by

$$\mathbf{\Delta}(s) := \{\delta(s, \mathbf{p}) \ : \ \mathbf{p} \in \mathbf{\Pi}\}. \tag{10.3}$$

Let $\mathbf{V}$ denote the vertices of $\mathbf{\Pi}$, i.e.,

$$\mathbf{V} := \left\{\mathbf{p} \ : \ p_i = p_i^+ \ \text{ or } \ p_i = p_i^-, \quad i = 1, 2, \cdots, l\right\} \tag{10.4}$$

and

$$\mathbf{\Delta}_{\mathrm{V}}(s) := \{\delta(s, \mathbf{p}) \ : \ \mathbf{p} \in \mathbf{V}\} := \{v_1(s), v_2(s), \cdots v_k(s)\}. \tag{10.5}$$

denote the set of *vertex polynomials*. Let $\bar{\mathbf{\Delta}}(s)$ denote the *convex hull* of the vertex polynomials $\{v_1(s), v_2(s), \cdots v_k(s)\}$:

$$\bar{\mathbf{\Delta}}(s) := \left\{ \sum_{i=1}^{i=k} \lambda_i v_i(s) : 0 \leq \lambda_i \leq 1, i = 1, 2 \cdots k \right\}.$$

The intersection of the sets $\mathbf{\Delta}(s)$ and $\bar{\mathbf{\Delta}}(s)$ contain the vertex polynomials $\mathbf{\Delta}_{\mathrm{V}}(s)$.

The Mapping Theorem deals with the image of $\mathbf{\Delta}(s)$ at $s = s^*$. Let $\mathbf{T}(s^*)$ denote the complex plane image of the set $\mathbf{T}(s)$ evaluated at $s = s^*$ and let *co* $\mathcal{P}$ denote the convex hull of a set of points $\mathcal{P}$ in the complex plane.

Theorem 10.1 (Mapping Theorem)
Under the assumption that $\delta_i(\mathbf{p})$ *are multilinear functions of* $\mathbf{p}$

$$\mathbf{\Delta}(s^*) \in co\ \mathbf{\Delta}_{\mathrm{V}}(s^*) = \bar{\mathbf{\Delta}}(s^*) \tag{10.6}$$

for each $s^* \in \mathbb{C}$.

Proof. For convenience we suppose that there are two uncertain parameters $\mathbf{p} := [p_1, p_2]$ and the uncertainty set $\mathbf{\Pi}$ is the rectangle $ABCD$ shown in Figure 10.2(a). Fixing $s = s^*$, we obtain $\delta(s^*, \mathbf{p})$ which maps $\mathbf{\Pi}$ to the complex plane. Let A', B', C', D' denote respectively the complex plane images of the vertices A, B, C, D under this mapping. Figures 10.2(b,c,d,e) show various configurations that can arise under this mapping. Now consider an arbitrary point I in $\mathbf{\Pi}$ and its complex plane image I'. The theorem is proved if we establish that I' is a convex combination of the complex numbers A', B', C', D'. We note that starting at an arbitrary vertex, say A, of $\mathbf{\Pi}$ we can reach I by moving along straight lines which are either edges of $\mathbf{\Pi}$ or are parallel to an edge of $\mathbf{\Pi}$. Thus, as shown in Figure 10.2(a), we move from A to E along the edge AB, and then from E to I along EF which is parallel to the edge AD. Because $\delta(s^*, \mathbf{p})$ is multilinear in the p_i it follows that the complex plane images of AB, EF, and CD, which are parallel to edges of $\mathbf{\Pi}$, are straight lines, respectively $A'B'$, $E'F'$, $C'D'$. Moreover, E' lies on the straight line $A'B'$, F' lies on the straight line $C'D'$, and I' lies on the straight line $E'F'$. Therefore, I' lies in the convex hull of $A'B'C'D'$.

The same reasoning works in higher dimensions. Any point in $\mathbf{\Pi}$ can be reached from a vertex by moving one coordinate at a time. In the image set this corresponds, because of multilinearity, to moving along straight lines joining vertices or convex combinations of vertices. By such movements we can never escape the convex hull of the vertices. The second equality holds by definition. ♣

We point out that the Mapping Theorem does not hold if $\mathbf{\Pi}$ is not an axis-parallel box since the image of the edge of an arbitrary polytope under a multilinear mapping is in general not a straight line. The Mapping Theorem will also not hold when the dependency on the parameters is polynomial rather than multilinear, because of the same reason.

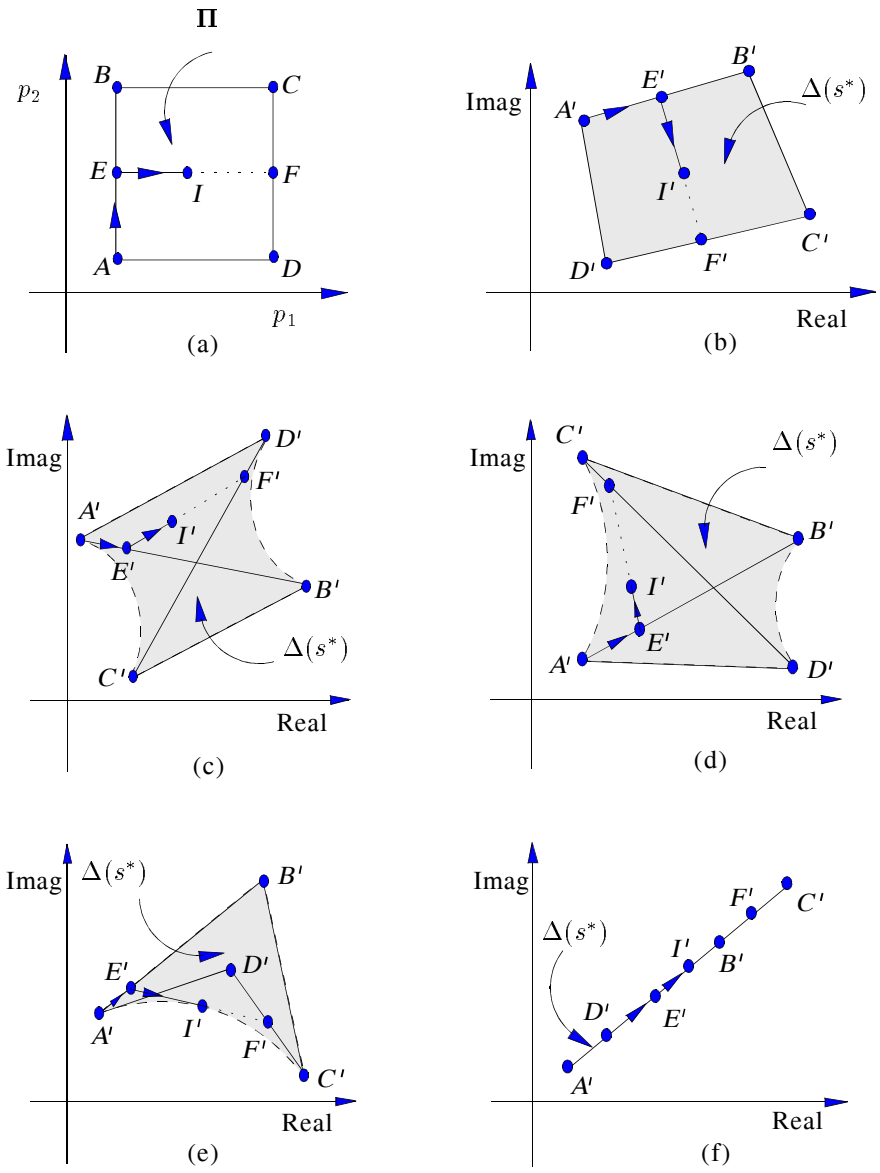

Figure 10.2. Proof of the Mapping Theorem

Example 10.1. Consider the multilinear interval polynomial

$$\delta(s, \mathbf{p}) = p_1 Q_1(s) + p_2 Q_2(s) + p_1 p_2 Q_3(s) + Q_4(s)$$

with

$$Q_1(s) = -6s + 2, \quad Q_2(s) = -5s - 1, \quad Q_3(s) = 10s + 3, \quad Q_4(s) = 7s + 5.$$

The parameter set $\mathbf{p}$ varies inside box $\mathbf{\Pi}$ depicted in Figure 10.3(a). The image set $\mathbf{\Delta}(s^*, \mathbf{p})$ of the family at $s^* = j1$ is shown in Figure 10.3(b). The convex hull of the image set $\mathbf{\Delta}(s^*)$ is also shown. This shows that

$$\mathbf{\Delta}(s^*, \mathbf{p}) \in co\ \mathbf{\Delta}_V(s^*, \mathbf{p}) = \bar{\mathbf{\Delta}}(s^*).$$

The four corners of the polygon in Figure 10.3(b) are the vertices of the image.

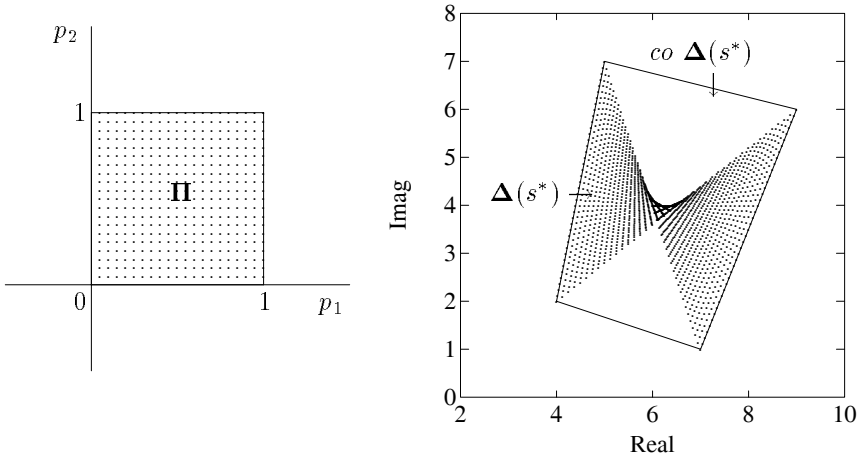

Figure 10.3. Parameter space, image set, and convex hull (Example 10.1)

This theorem shows us that the image set of the multilinear family $\mathbf{\Delta}(s)$ can always be approximated by overbounding it with the image of the polytopic family $\bar{\mathbf{\Delta}}(s)$. This approximation is extremely useful. In the next section we show how it allows us to determine robust stability and stability margins quantitatively.

10.3 ROBUST STABILITY VIA THE MAPPING THEOREM

As we have seen in earlier chapters, the robust stability of a parametrized family of polynomials can be determined by verifying that the image set evaluated at each point of the stability boundary excludes the origin. The Mapping Theorem shows us that the image set of a multilinear interval polynomial family is contained in the convex hull of the vertices. Obviously a sufficient condition for the entire image set to exclude zero is that the convex hull exclude zero. Since the image set $\mathbf{\Delta}(s^*)$ is overbounded by the convex hull of $\mathbf{\Delta}_{\mathrm{V}}(s^*)$, this suggests that the stability of the *multilinear* set $\mathbf{\Delta}(s)$ can be guaranteed by solving the easier problem of verifying the stability of the *polytopic* set $\bar{\mathbf{\Delta}}(s)$. We develop this idea in this section.

As usual, let $\mathcal{S}$, an open set in the complex plane, be the stability region. Introduce the set of edges $\mathbf{E}(s)$ of the polytope $\bar{\mathbf{\Delta}}(s)$:

$$\mathbf{E}(s) := \{\lambda v_i(s) + (1-\lambda)v_j(s) \ : \ v_i(s), v_j(s) \in \mathbf{\Delta}_{\mathrm{V}}(s)\}\,. \tag{10.7}$$

To proceed, we make some standing assumptions about the families $\mathbf{\Delta}(s)$ and $\bar{\mathbf{\Delta}}(s)$.

Assumption 10.1.

1) Every polynomial in $\mathbf{\Delta}(s)$ and $\bar{\mathbf{\Delta}}(s)$ is of the same degree.

2) $0 \notin \bar{\mathbf{\Delta}}(s_0)$ for some $s_0 \in \partial\mathcal{S}$.

3) At least one polynomial in $\mathbf{\Delta}(s)$ is stable.

Theorem 10.2 *Under the above assumptions, $\mathbf{\Delta}(s)$ is stable with respect to $\mathcal{S}$ if $\bar{\mathbf{\Delta}}(s)$ and equivalently $\mathbf{E}(s)$ is stable with respect to $\mathcal{S}$.*

Proof. Since the degree remains invariant, we may apply the Boundary Crossing Theorem (Chapter 1). Thus, $\mathbf{\Delta}(s)$ can be unstable if and only if $0 \in \mathbf{\Delta}(s^*)$ for some $s^* \in \partial\mathcal{S}$. By assumption, there exist $s_0 \in \partial\mathcal{S}$ such that

$$0 \notin \bar{\mathbf{\Delta}}(s_0) = co\ \mathbf{E}(s_0).$$

By the Mapping Theorem

$$\mathbf{\Delta}(s^*) \subset \bar{\mathbf{\Delta}}(s^*) = co\ \mathbf{E}(s^*).$$

Therefore, by continuity of the image set on s, $0 \in \mathbf{\Delta}(s^*)$ must imply the existence of $\bar{s} \in \partial\mathcal{S}$ such that $0 \in \mathbf{E}(\bar{s})$. This contradicts the stability of $\bar{\mathbf{\Delta}}(s)$ and of $\mathbf{E}(s)$. ♣

This theorem is just a statement of the fact that the origin can enter the image set $\mathbf{\Delta}(s^*)$ only by piercing one of the edges $\mathbf{E}(\bar{s})$. Nevertheless the result is rather remarkable in view of the fact that the set $\bar{\mathbf{\Delta}}(s)$ does not necessarily contain, nor is it contained in, the set $\mathbf{\Delta}(s)$. In fact the inverse image of $\mathbf{E}(s)$ in the parameter space will in general include points outside $\mathbf{\Pi}$. The theorem works because the *image set*

$\boldsymbol{\Delta}(s^*)$ *is overbounded* by $\bar{\boldsymbol{\Delta}}(s)$ at every point $s^* \in \partial\mathcal{S}$. This in turn happens because the Mapping Theorem guarantees that $\boldsymbol{\Delta}(s^*)$ is "concave" or bulges inward.

The test set $\bar{\boldsymbol{\Delta}}(s)$ or its edges $\mathbf{E}(s)$ are linearly parametrized families of polynomials. Thus, the above theorem allows us to test a multilinear interval family using all the techniques available in the linear case.

Example 10.2. Consider the multilinear interval polynomial

$$\delta(s, \mathbf{p}) = p_1 Q_1(s) + p_2 Q_2(s) + p_1 p_2 Q_3(s)$$

where

$$p_1 \in [1, 2], \quad p_2 \in [3, 4]$$

and

$$\begin{aligned} Q_1(s) &= s^4 + 4.3s^3 + 6.2s^2 + 3.5s + 0.6, \\ Q_2(s) &= s^4 + s^3 + 0.32s^2 + 0.038s + 0.0015, \\ Q_3(s) &= s^4 + 3.5s^3 + 3.56s^2 + 1.18s + 0.12. \end{aligned}$$

The edges of this system are,

$$\mathbf{E}(s) = \{E_i(s), \quad i = 1, 2, 3, 4\}$$

with

$$\begin{aligned} E_1(s) &= \left[\lambda p_1^- + (1-\lambda)p_1^+\right] Q_1(s) + p_2^- Q_2(s) + \left[\lambda p_1^- + (1-\lambda)p_1^+\right] p_2^- Q_3(s) \\ &= \lambda \left[p_1^- Q_1(s) + p_2^- Q_2(s) + p_1^- p_2^- Q_3(s)\right] \\ &\qquad +(1-\lambda)\left[p_1^+ Q_1(s) + p_2^- Q_2(s) + p_1^+ p_2^- Q_3(s)\right] \\ E_2(s) &= \left[\lambda p_1^- + (1-\lambda)p_1^+\right] Q_1(s) + p_2^+ Q_2(s) + \left[\lambda p_1^- + (1-\lambda)p_1^+\right] p_2^+ Q_3(s) \\ &= \lambda \left[p_1^- Q_1(s) + p_2^+ Q_2(s) + p_1^- p_2^+ Q_3(s)\right] \\ &\qquad +(1-\lambda)\left[p_1^+ Q_1(s) + p_2^+ Q_2(s) + p_1^+ p_2^+ Q_3(s)\right] \\ E_3(s) &= p_1^- Q_1(s) + \left[\lambda p_2^- + (1-\lambda)p_2^+\right] Q_2(s) + \left[\lambda p_2^- + (1-\lambda)p_2^+\right] p_1^- Q_3(s) \\ &= \lambda \left[p_1^- Q_1(s) + p_2^- Q_2(s) + p_1^- p_2^- Q_3(s)\right] \\ &\qquad +(1-\lambda)\left[p_1^- Q_1(s) + p_2^+ Q_2(s) + p_1^- p_2^+ Q_3(s)\right] \\ E_4(s) &= p_1^+ Q_1(s) + \left[\lambda p_2^- + (1-\lambda)p_2^+\right] Q_2(s) + \left[\lambda p_2^- + (1-\lambda)p_2^+\right] p_1^+ Q_3(s) \\ &= \lambda \left[p_1^+ Q_1(s) + p_2^- Q_2(s) + p_1^+ p_2^- Q_3(s)\right] \\ &\qquad +(1-\lambda)\left[p_1^+ Q_1(s) + p_2^+ Q_2(s) + p_1^+ p_2^+ Q_3(s)\right]. \end{aligned}$$

The stability of $\mathbf{E}(s)$ can be tested simply by applying the Segment Lemma (Chapter 2). Here, all edges in $\mathbf{E}(s)$ are found to be stable.

Bounded Phase Condition

An alternative way of stating Theorem 10.2 is to use the Bounded Phase Condition. Let $\Phi_{\mathbf{\Delta}_V}(s^*)$ equal the angle subtended at the origin by the points $\mathbf{\Delta}_V(s^*)$. Obviously, the stability of $\mathbf{E}(s)$ is equivalent, under the Assumptions 10.1, to the origin being excluded from $\bar{\mathbf{\Delta}}(s^*)$ for all $s^* \in \partial\mathcal{S}$, and this in turn is equivalent to the condition that the phase spread be less than π radians. Accordingly we have the following theorem.

Theorem 10.3 *Under the assumptions 10.1, $\mathbf{\Delta}(s)$ is stable with respect to $\mathcal{S}$ if*

$$\Phi_{\bar{\mathbf{\Delta}}_V}(s^*) < \pi, \qquad \text{for all } s^* \in \partial\mathcal{S}. \tag{10.8}$$

Example 10.3. Let us return to Example 10.2 and determine the robust stability of this multilinear interval polynomial by applying the Bounded Phase Condition. We first construct the set of vertex polynomials corresponding to the vertices of the parameter space box $\mathbf{\Pi} = [p_1,\ p_2]$.

$$\begin{aligned}
v_1(s) &= 7s^4 + 17.8s^3 + 17.84s^2 + 7.154s + 0.9645\\
v_2(s) &= 11s^4 + 32.6s^3 + 34.72s^2 + 14.194s + 1.9245\\
v_3(s) &= 9s^4 + 22.3s^3 + 21.72s^2 + 8.372s + 1.086\\
v_4(s) &= 14s^4 + 40.6s^3 + 42.16s^2 + 16.592s + 2.166.
\end{aligned}$$

The maximum phase difference over the vertex set at each frequency ω is computed as follows:

$$\Phi_{\bar{\mathbf{\Delta}}_V} = \sup_{i=2,3,4} \arg \frac{v_i(j\omega)}{v_1(j\omega)} - \inf_{i=2,3,4} \arg \frac{v_i(j\omega)}{v_1(j\omega)}.$$

The plot of the above phase function for all ω is shown in Figure 10.4. We find that the maximum phase difference over the vertex set does not reach 180° for any ω. Thus we conclude that the given multilinear polynomial family is Hurwitz stable.

10.3.1 Refinement of the Convex Hull Approximation

Since the stability of the set $\bar{\mathbf{\Delta}}(s)$ or $\mathbf{E}(s)$ is only a sufficient condition for the stability of $\mathbf{\Delta}(s)$, it can happen that $\mathbf{E}(s)$ is unstable but $\mathbf{\Delta}(s)$ is stable. In this case the sufficient condition given by the theorem can be tightened by introducing additional vertices. We illustrate this in the accompanying figures. Consider the multilinear polynomial

$$Q_0(s) + p_1Q_1(s) + p_2Q_2(s) + p_1p_2Q_3(s)$$

where

$$\begin{aligned}
Q_0(s) &= s^4 + s^3 + 2s^2 + s + 2,\\
Q_1(s) &= 2s^4 + 3s^3 + 4s^2 + s + 1,\\
Q_2(s) &= 1.5s^4 + 1.5s^3 + 3s^2 + s + 0.5,\\
Q_3(s) &= 3s^4 + 0.5s^3 + 1.5s^2 + 2s + 2
\end{aligned}$$

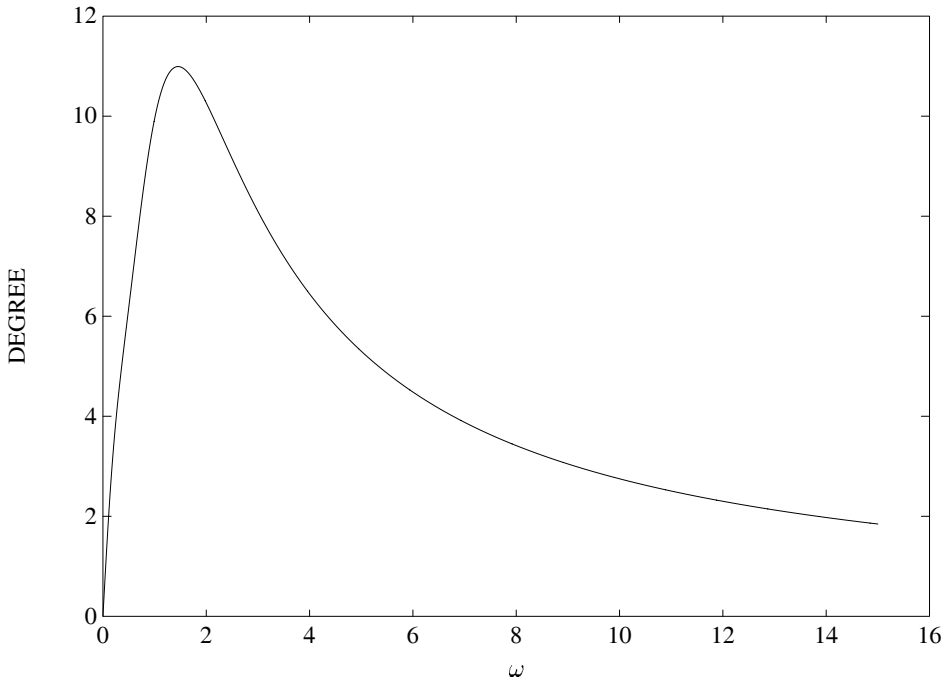

Figure 10.4. Maximum phase difference (Example 10.3)

and the parameter $\mathbf{p}$ varies within the box shown in Figure 10.5.

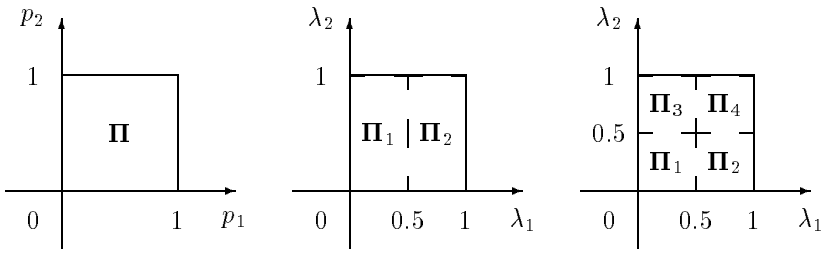

Figure 10.5. Additional vertices in parameter space

As shown in Figure 10.5 one may introduce additional vertices in the parameter

space. The corresponding image sets at $\omega = 0.85$ are shown in Figures 10.6, 10.7, and 10.8. We see that this amounts to decomposing the parameter box as a union of smaller boxes:

$$\mathbf{\Pi} = \bigcup_{i=1}^{t} \mathbf{\Pi}_i. \tag{10.9}$$

If $\mathbf{V}_i$ and $\mathbf{E}_i(z)$ denote the corresponding vertices and edges, we have

$$co\ \mathbf{\Delta}(z^*) \subset \bigcup_{i=1}^{t} \bar{\mathbf{\Delta}}_{\mathbf{V}_i}(z^*) = \bigcup_{i=1}^{t} co\ \mathbf{E}_i(z^*) \tag{10.10}$$

and therefore the stability of the set of line segments $\bigcup_{i=1}^{m} \mathbf{E}_i(z)$ would imply that of $\mathbf{\Delta}(z)$. We can see from Figures 10.7 and 10.8 that the nonconvex set $\bigcup_{i=1}^{m} \mathbf{E}_i(z^*)$ approximates $\mathbf{\Delta}(z^*)$ more closely as the number t of polytopes $\mathbf{\Pi}_i$ increases. It is clear therefore that the sufficient condition given here can be improved to any desired level of accuracy by checking the stability of smaller convex hulls.

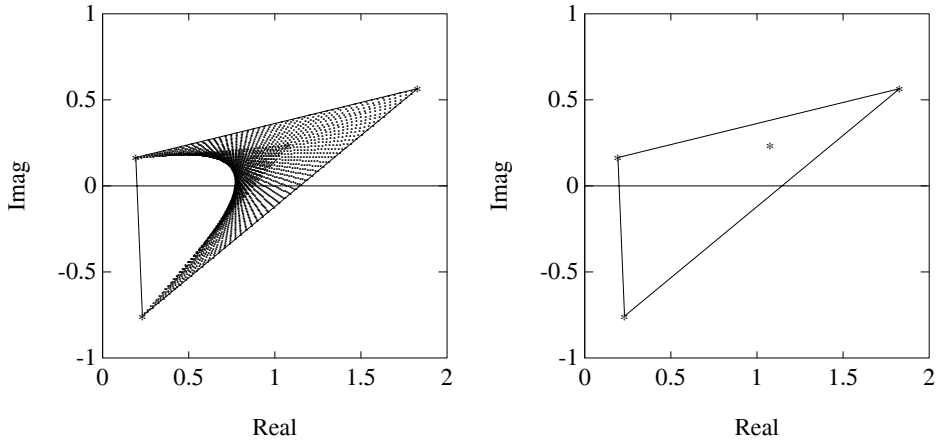

Figure 10.6. Image set and convex hull ($\omega = 0.85$)

10.4 MULTILINEAR INTERVAL SYSTEMS

In this section we consider system transfer functions which are ratios of multilinear interval polynomials. We call such systems *multilinear interval systems*. Our objective is to analyze feedback control systems containing such multilinear interval plants. In addition to determining robust stability, we are interested in calculating various types of stability and performance margins for such systems. Let $M(s)$

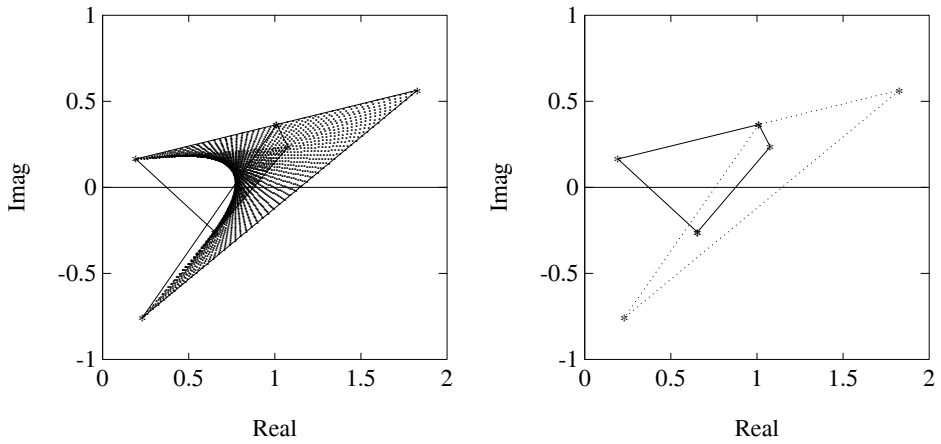

Figure 10.7. Image set and convex hull (2 partitions) ($\omega = 0.85$)

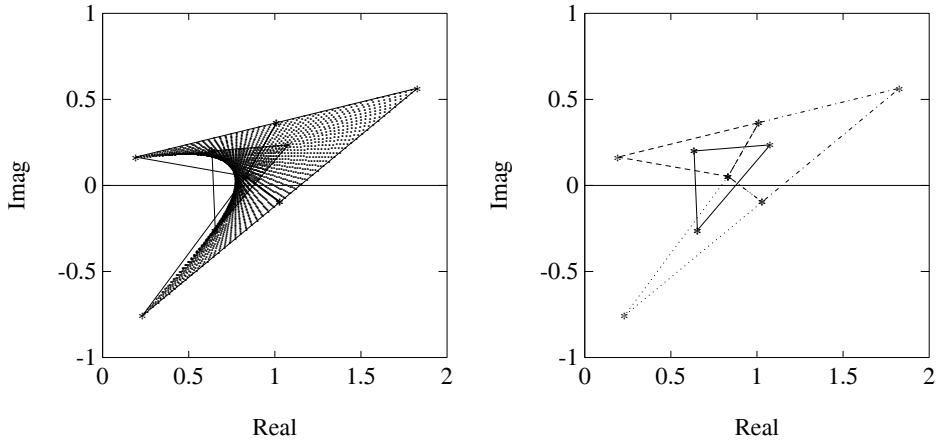

Figure 10.8. Image set and convex hull (4 partitions) ($\omega = 0.85$)

denote a transfer function which depends on the uncertain, interval, independent parameters $\mathbf{q}$ and $\mathbf{r}$:

$$M(s) = M(s, \mathbf{q}, \mathbf{r}) = \frac{N(s, \mathbf{q})}{D(s, \mathbf{r})}. \tag{10.11}$$

We assume that $N(s,\mathbf{q})$ and $D(s,\mathbf{r})$ are multilinear interval polynomials and $\mathbf{q}$ and $\mathbf{r}$ lie in axis parallel boxes $\mathbf{Q}$ and $\mathbf{R}$ respectively. Let

$$\mathbf{N}(s) := \{N(s,\mathbf{q}) : \mathbf{q} \in \mathbf{Q}\}$$

$$\mathbf{D}(s) := \{D(s,\mathbf{r}) : \mathbf{r} \in \mathbf{R}\}$$

and write

$$\mathbf{M}(s) := \left\{ \frac{N(s,\mathbf{q})}{D(s,\mathbf{r})} : \mathbf{q} \in \mathbf{Q}, \mathbf{r} \in \mathbf{R} \right\} := \frac{\mathbf{N}(s)}{\mathbf{D}(s)}.$$

Now, suppose that the multilinear interval plant we have described is part of a control system. For robustness studies, it is important that we obtain an assessment of the worst case stability margins and performance measures of the system over the uncertainty set $\mathbf{\Pi} := \mathbf{Q} \times \mathbf{R}$. We shall show here that by using the Mapping Theorem we can replace the family $\mathbf{M}(s)$ by a polytopic family $\bar{\mathbf{M}}(s)$ which has the property that any worst case stability or performance margin that is calculated for the family $\bar{\mathbf{M}}(s)$ serves as a corresponding *guaranteed* margin for the family $\mathbf{M}(s)$. The advantage that we gain is that worst case stability and performance margins can be evaluated *easily and exactly* for the family $\bar{\mathbf{M}}(s)$ since it is polytopic.

Construction of $\bar{\mathbf{M}}(s)$

Let $\mathbf{V}_Q$ denote the vertex set of $\mathbf{Q}$, $\mathbf{N}_{\mathrm{V}}(s)$ the corresponding vertex polynomials

$$\mathbf{N}_{\mathrm{V}}(s) := \{N(s,\mathbf{q}) : \mathbf{q} \in \mathbf{V}_Q\}$$

and $\bar{\mathbf{N}}(s)$ the convex hull of $\mathbf{N}_{\mathrm{V}}(s)$:

$$\bar{\mathbf{N}}(s) := \{\lambda N_i(s) + (1-\lambda)N_j(s) : N_i(s), N_j(s) \in \mathbf{N}_{\mathrm{V}}(s), \quad \lambda \in [0,1]\}.$$

In an identical manner we can define the sets $\mathbf{V}_R, \mathbf{D}_{\mathrm{V}}(s)$ and $\bar{\mathbf{D}}(s)$. Now we can introduce the transfer function sets

$$\mathbf{M}_{\mathrm{V}}(s) := \frac{\mathbf{N}_{\mathrm{V}}(s)}{\mathbf{D}_{\mathrm{V}}(s)}$$

and

$$\bar{\mathbf{M}}(s) := \frac{\bar{\mathbf{N}}(s)}{\bar{\mathbf{D}}(s)}.$$

From the Mapping Theorem we know that at every point $s^* \in \mathbb{C}$ the image sets of $\mathbf{N}(s)$ and $\mathbf{D}(s)$ contain the image of the vertices and are overbounded respectively by the images of the polytopic families $\bar{\mathbf{N}}(s)$ and $\bar{\mathbf{D}}(s)$ respectively:

$$\mathbf{N}_{\mathrm{V}}(s^*) \subset \mathbf{N}(s^*) \subset \bar{\mathbf{N}}(s^*)$$

$$\mathbf{D}_{\mathrm{V}}(s^*) \subset \mathbf{D}(s^*) \subset \bar{\mathbf{D}}(s^*).$$

As usual we assume that $0 \notin \bar{\mathbf{D}}(s^*)$ so that the above sets are well-defined. From the above it follows that the image set of $\mathbf{M}(s)$ contains the image of the vertices $\mathbf{M}_V(s)$ and is also overbounded by the image of $\bar{\mathbf{M}}(s)$.

Lemma 10.1

$$\mathbf{M}_{\mathrm{V}}(s^*) \subset \mathbf{M}(s^*) \subset \bar{\mathbf{M}}(s^*).$$

This result suggests that by substituting the multilinear interval family $\mathbf{M}(s)$ by the polytopic family $\bar{\mathbf{M}}(s)$ in a control system we can calculate a lower bound on the worst case stability margin or performance margin of the system. To state this more precisely suppose that $M(s) \in \mathbf{M}(s)$ is part of a feedback control system. We will assume that the order of the closed loop system, i.e. the degree of the characteristic polynomial, remains invariant over $M(s) \in \mathbf{M}(s)$ and also over $M(s) \in \bar{\mathbf{M}}(s)$. As usual let $\mathcal{S}$ denote a stability region that is relevant to the system under consideration.

Theorem 10.4 *Under the assumption of invariant order, robust stability of the control system holds with $M(s) \in \mathbf{M}(s)$ if it holds with $M(s) \in \bar{\mathbf{M}}(s)$.*

The proof of this result follows immediately from the image set bounding property of the set $\bar{\mathbf{M}}(s)$ evaluated at points s^* on the stability boundary $\partial\mathcal{S}$, which is stated in the Lemma above. The result holds for arbitrary stability regions with Hurwitz and Schur stability being particular cases.

Suppose now that we are dealing with a continuous time control system and that we have verified the robust Hurwitz stability of the system with $M(s) \in \bar{\mathbf{M}}(s)$. The next important issue is to determine the performance of the system in some suitably defined meaningful way. The usual measures of performance are gain margin, phase margin, time-delay tolerance, H_∞ stability or performance margins, parametric stability radius in the parameter $\mathbf{p}$ and nonlinear sector bounded stability margins as in the Lur'e or Popov problems treated in Chapter 8. Let μ refer to one of these performance measures and let us assume that increasing values of μ reflect better performance. Let μ^* denote the worst case value of μ over the set $M(s) \in \mathbf{M}(s)$, $\underline{\mu}$ denote the worst case value of μ over $M(s) \in \bar{\mathbf{M}}(s)$ and $\bar{\mu}$ denote the worst case value of μ over the vertex set $M(s) \in \mathbf{M}_{\mathrm{V}}(s)$. Then it is obviously true that

$$\underline{\mu} \leq \mu^* \leq \bar{\mu}.$$

Since $\bar{\mathbf{M}}(s)$ is a polytopic set, we can calculate $\underline{\mu}$ exactly. As in the Mapping Theorem, this lower bound can be increased by subdividing the box $\mathbf{\Pi}$ into smaller boxes. On the other hand, $\bar{\mu}$ can be calculated very easily because it is the minimum of μ evaluated over the vertex points. By subdividing the box $\mathbf{\Pi}$, this upper bound can be decreased and the gap between the upper and lower bounds can be reduced to arbitrarily small values by introducing additional vertices to refine the convex hull approximation. Thus the worst case performance over the parameter set $\mathbf{\Pi}$, also known as robust performance, can be accurately determined. In the following section we illustrate this procedure for estimating worst case performance in greater detail with numerical examples.

10.5 EXAMPLES

We illustrate the procedure for calculating robust stability and performance margins by examples.

10.5.1 Parametric Stability Margin

For a given uncertainty set $\mathbf{\Pi}$, we can verify robust stability using the Mapping Theorem. In applications, it is of interest to know how large $\mathbf{\Pi}$ can be without losing stability. This problem can also be solved using the convex hull approximation. We illustrate this with an example.

Example 10.4. Consider the discrete time feedback system as shown Figure 10.9.

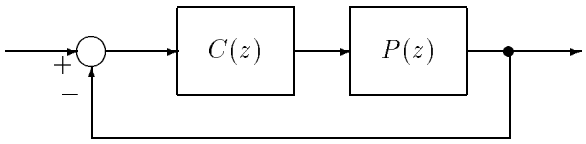

Figure 10.9. Discrete-time feedback systems (Example 10.4)

$$P(z) := \frac{P_1(z)}{P_2(z)} = \frac{z - z_0}{(z - p_1)(z - p_2)} \quad \text{and} \quad C(z) := \frac{C_1(z)}{C_2(z)} = \frac{z + 1.29}{z - 0.5}$$

and let the set of system parameters $\mathbf{p} = [z_0, p_1, p_2]$ vary in a box whose size varies with a dilation parameter ϵ as follows:

$$\begin{aligned} z_0 &\in [z_0^-, z_0^+] = [0.5 - \epsilon, 0.5 + \epsilon] \\ p_1 &\in [p_1^-, p_1^+] = [1.0 - \epsilon, 1.0 + \epsilon] \\ p_2 &\in [p_2^-, p_2^+] = [-1.0 - \epsilon, -1.0 + \epsilon]. \end{aligned}$$

The characteristic polynomial of the system is

$$\begin{aligned} \delta(z, \mathbf{p}) = z^3 + (0.5 - p_1 - p_2)z^2 + (1.29 + 0.5p_1 + 0.5p_2 + p_1p_2 - z_0)z \\ -0.5p_1p_2 - 1.29z_0. \end{aligned}$$

We see that the coefficients are multilinear functions of $\mathbf{p}$. Therefore Theorem 10.4 may be applied. We verify that the following member of the family is Schur stable:

$$\delta(z, \mathbf{p} = [0.5, 1, -1]) = z^3 + 0.5z^2 - 0.21z - 0.145.$$

We would like to determine the largest sized box for which we have closed loop stability. This can be regarded as the worst case parametric stability margin ϵ^* of

the family. Using a simple bisection algorithm, we find that a lower bound $\underline{\epsilon}$ on the the parametric stability margin ϵ^* is 0.125 as shown in Figure 10.10.

On the other hand we can get an upper bound $\bar{\epsilon}$ from the vertices. This gives $\bar{\epsilon} = 0.125$, which is the same as the lower bound, and thus the true value in this case.

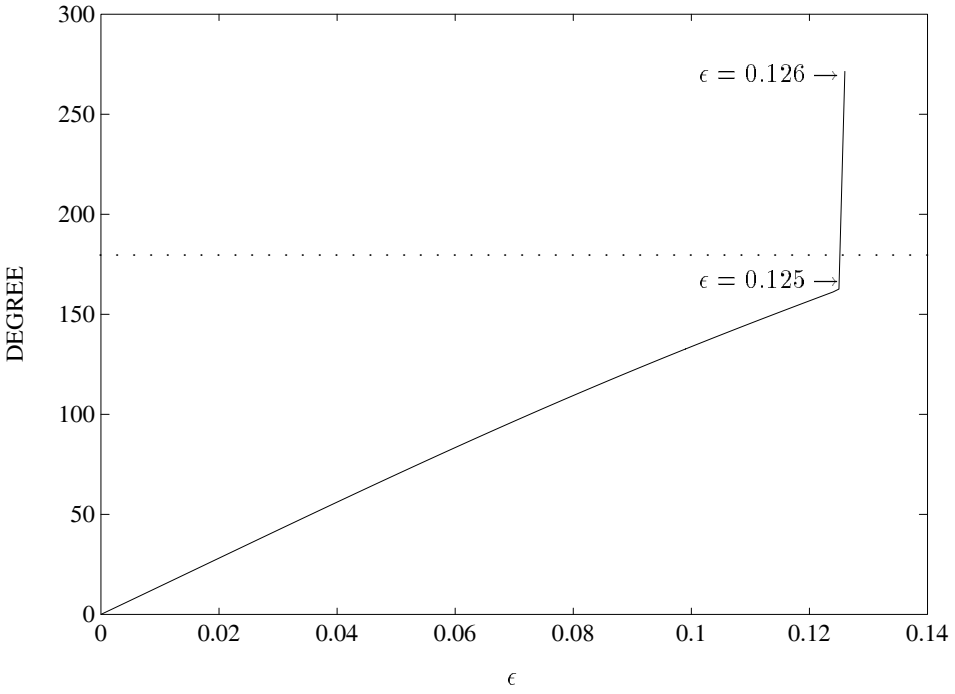

Figure 10.10. Maximum phase difference (Example 10.4)

10.5.2 Robust Gain, Phase, Time-delay and H_∞ Stability Margins

In this section we focus on a control system example and show how robust performance measured in each of the above ways, over a multilinear parameter set, can be estimated from the polytopic overbounding method discussed earlier.

Example 10.5. Consider the control system block diagram shown in Figure 10.11.

Let

$$F(s) := \frac{F_1(s)}{F_2(s)} = \frac{s+1}{s+2} \quad \text{and} \quad P(s) := \frac{P_1(s)}{P_2(s)} = \frac{s+p_1}{s^2+p_2 s+4}$$

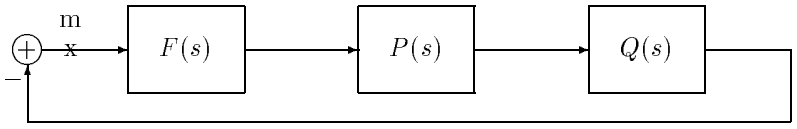

Figure 10.11. A multilinear interval control system (Example 10.5)

$$Q(s) := \frac{Q_1(s)}{Q_2(s)} = \frac{s + p_3}{s^3 + 3s^2 + p_4 s + 0.1}$$

where

$$p_1 \in [2.9, 3.1] =: [p_1^-, p_1^+] \qquad p_2 \in [1.9, 2.1] =: [p_2^-, p_2^+]$$
$$p_3 \in [4.9, 5.1] =: [p_3^-, p_3^+] \qquad p_4 \in [1.9, 2.1] =: [p_4^-, p_4^+].$$

The family of characteristic polynomials is

$$\mathbf{\Delta}(s, \mathbf{p}) = \{F_2(s)P_2(s)Q_2(s) + F_1(s)P_1(s)Q_1(s) \ : \ \mathbf{p} \in \mathbf{\Pi}\}$$

where the parameter space box is given as

$$\mathbf{\Pi} := \left\{\mathbf{p} : p_i \in [p_i^-, p_i^+] \ \ i = 1, 2, 3, 4\right\}.$$

Now we construct the 16 vertex polynomials corresponding to the vertex set $\mathbf{V}$ of $\mathbf{\Pi}$:

$$\mathbf{\Delta}_{\mathrm{V}}(s) = \{v(s, \mathbf{p}) \ : \ \mathbf{p} \in \mathbf{V}\} = \{v_i(s) = v_i(s, \mathbf{p}), \quad i = 1, 2, \cdots, 16\}.$$

The vertex polynomials $v_i(s)$ can be written down by setting $\mathbf{p}$ to a vertex value. For example:

$$\begin{aligned} v_1(s) &= v(s, p_1^+, p_2^+, p_3^+, p_4^+) \\ &= \underbrace{(s+2)(s^2 + p_2^+ s + 4)(s^3 + 3s^2 + p_4^+ s + 0.1)}_{V_1^D(s)} + \underbrace{(s+1)(s+p_1^+)(s+p_3^+)}_{V_1^N(s)}. \end{aligned}$$

Similarly, we can write $v_2(s)$, $\cdots$, v_{16}.

(a) To determine the worst case upper gain margin L^* over the parameter set, we replace the vertex polynomials as follows:

$$V_i(s, L) = V_i^D(s) + (1 + L)V_i^N(s), \quad i = 1, 2, \cdots, 16.$$

Now find the maximum phase difference over the entire set of vertex polynomials $\mathbf{\Delta}_{\mathrm{V}}(j\omega)$ for a fixed ω with a fixed L:

$$\Phi_{\mathbf{\Delta}_{\mathrm{V}}}(\omega, L) = \sup_{i, i \neq k} \arg \frac{V_i(j\omega, L)}{V_k(j\omega, L)} - \inf_{i, i \neq k} \arg \frac{V_i(j\omega, L)}{V_k(j\omega, L)}$$

where k is an arbitrary integer, $1 \leq k \leq 16$, and $i = 1, 2, \cdots, 16$. Then a lower bound $\underline{L}$ on the worst case gain margin is obtained by determining the largest real positive value of L such that all the edges connecting the vertices in $\mathbf{\Delta}_{\mathrm{V}}(s)$ remain Hurwitz. Equivalently, by the Bounded Phase Condition we have

$$\underline{L} = \inf_{L \geq 0} \left\{ L \ : \ \sup_{\omega} \Phi_{\mathbf{\Delta}_{\mathrm{V}}}(\omega, L) = 180^{\circ} \right\}.$$

Figure 10.12 shows that the maximum phase differences over the vertex set for each frequency ω for $L = 0$.

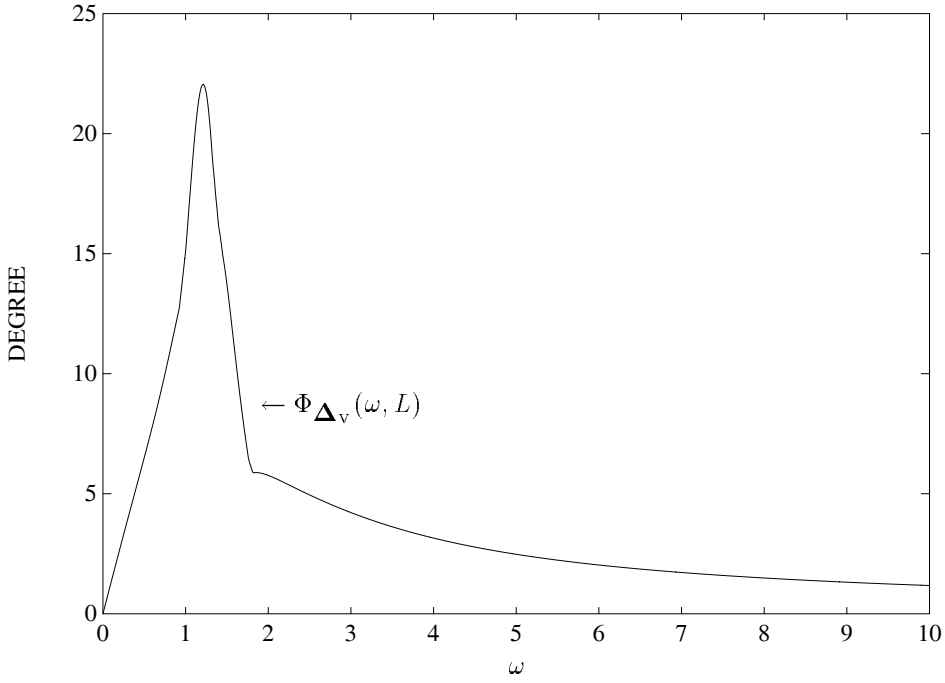

Figure 10.12. $\Phi_{\mathbf{\Delta}_{\mathrm{V}}}(\omega, L)$ vs. ω $(L = 0)$ (Example 10.5(a))

The figure shows that the maximum phase difference over vertices $\Phi_{\mathbf{\Delta}_{\mathrm{V}}}(\omega, L)$ does not reach 180° for any ω. This means that a larger value L is allowed. Figure 10.13 shows the plot of the maximum phase difference over the vertices and over all frequency in terms of L. From this we find that for $\underline{L} = 0.658$ there exists a frequency ω that results in $\Phi_{\mathbf{\Delta}_{\mathrm{V}}}(\omega, L) = 180^{\circ}$. Therefore,

$$\underline{L} \approx 0.658$$

On the other hand, we can determine an upper bound on L^* by finding the smallest gain margin over the vertex set. This turns out to be $\bar{L} = 0.658$ which is the same as $\underline{L}$, and therefore the exact margin in this case.

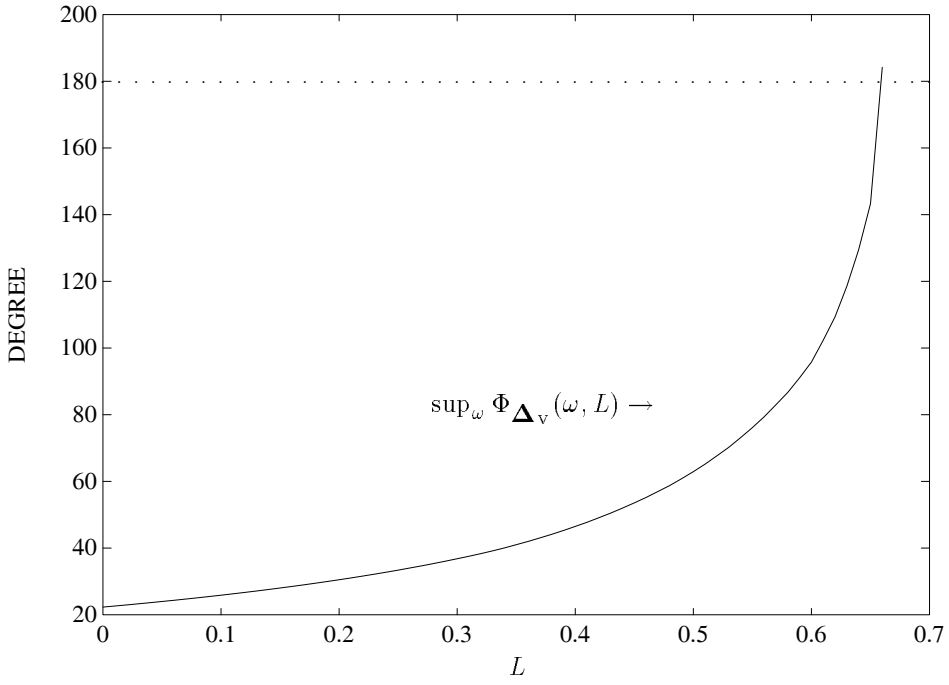

Figure 10.13. $\sup_\omega \Phi_{\mathbf{\Delta}_V}(\omega, L)$ vs. L (Example 10.5(a))

(b) To determine the worst case phase margin θ^* we modify each vertex polynomial as follows:

$$V_i(s, \theta) = V_i^D(s) + e^{j\theta} V_i^N(s), \quad i = 1, 2, \cdots, 16.$$

Then a lower bound $\underline{\theta}$ on θ^* can be obtained by finding the largest value of θ such that the Bounded Phase Condition is satisfied. Equivalently,

$$\underline{\theta} = \inf_{\theta \geq 0} \left\{ \theta \ : \ \sup_\omega \Phi_{\mathbf{\Delta}_V}(\omega, \theta) = 180^\circ \right\}.$$

Figure 10.14 shows the plot of the maximum phase difference over the vertices and over all ω in terms of θ. From this, we find that for $\underline{\theta} = 31.6273^\circ$ there exists ω that results in $\Phi_{\mathbf{\Delta}_V}(\omega, \theta) = 180^\circ$. Thus,

$$\underline{\theta} \approx 31.6273^\circ.$$

On the other hand, from the vertex systems we also get an upper bound $\bar{\theta} \approx 31.6273°$, which is the same as for $\underline{\theta}$, and hence $31.6273°$ is the true margin in this case.

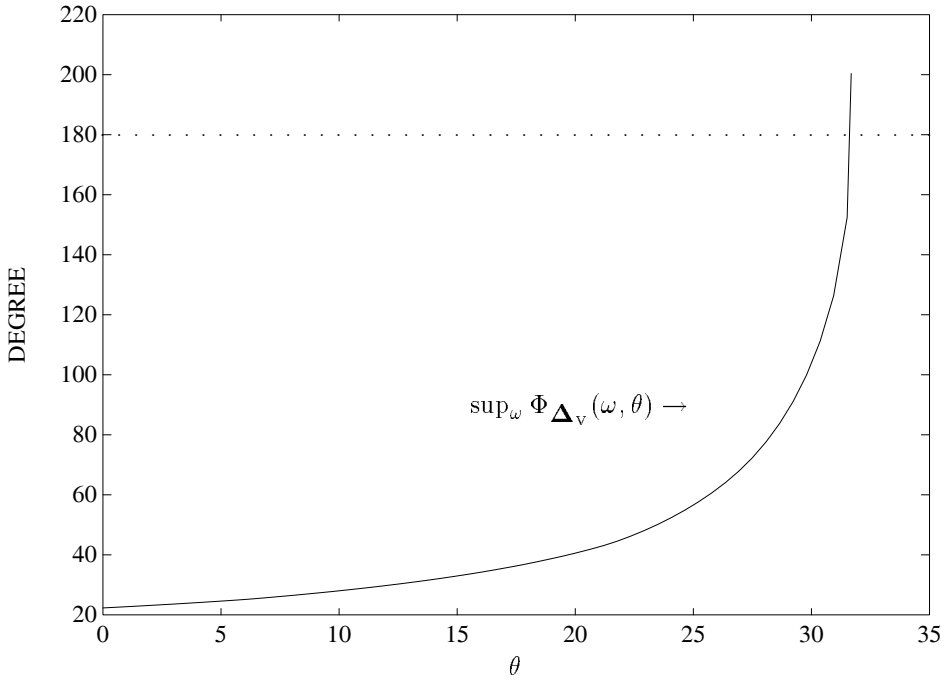

Figure 10.14. $\sup_\omega \Phi_{\mathbf{\Delta}_{\rm v}}(\omega, \theta)$ vs. θ (Example 10.5(b))

(c) To determine the worst case time delay margin T^*, we replace each vertex polynomial as follows:

$$V_i(s,T) = V_i^D(s) + e^{-j\omega T} V_i^N(s), \quad i = 1, 2, \cdots, 16.$$

A lower bound $\underline{T}$ on T^* is obtained by selecting the largest value of T such that the Bounded Phase Condition is satisfied. Equivalently,

$$\underline{T} = \inf_{T \geq 0} \left\{ T \ : \ \sup_{\omega} \Phi_{\mathbf{\Delta}_{\rm v}}(\omega, T) = 180° \right\}.$$

Figure 10.15 shows that at $T = 0.56$ there exists ω that results in $\Phi_{\mathbf{\Delta}_{\rm v}}(\omega, T) = 180°$. Thus we have

$$\underline{T} = 0.56 \ \text{ sec.}$$

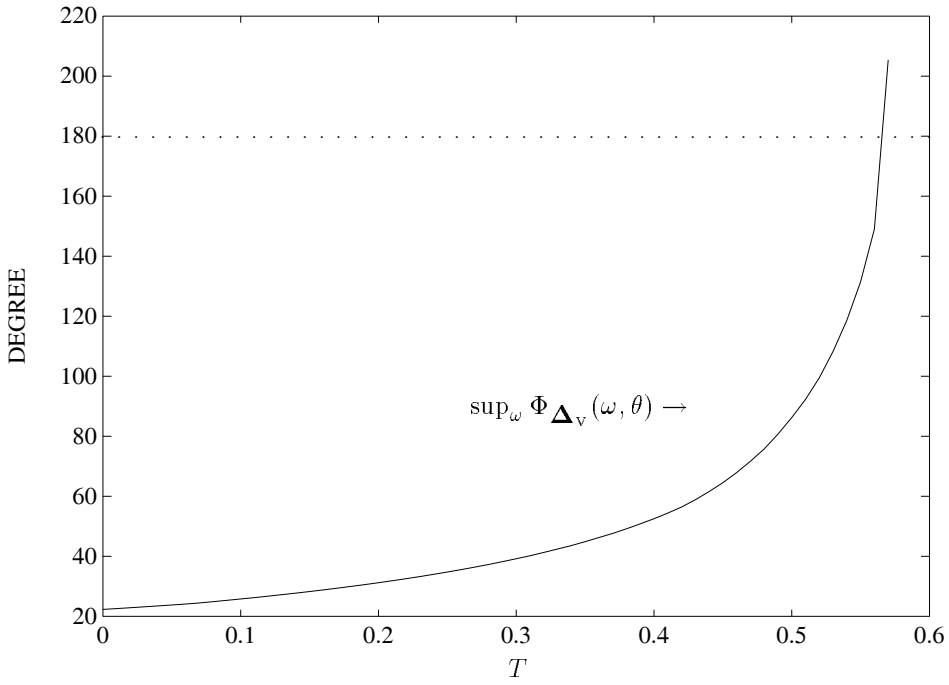

Figure 10.15. $\sup_\omega \Phi_{\mathbf{\Delta}_v}(\omega, \theta)$ vs. T (Example 10.5(c))

(d) To determine the worst case H_∞ stability margin, let us consider the case of additive perturbation where the H_∞ uncertainty block is connected around the two cascaded interval plants as shown in Figure 10.16.

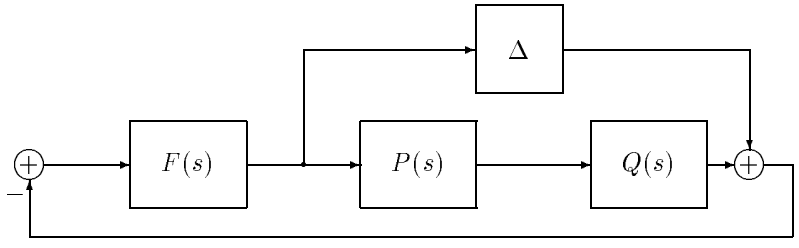

Figure 10.16. A multilinear interval system with H_∞ uncertainty (Example 10.5(d))

Then from

$$\left\| F(s)\left(1+F(s)P(s)Q(s)\right)^{-1}\right\|_{\infty} < \frac{1}{\beta},$$

we have the condition that

$$F_2(s)P_2(s)Q_2(s) + F_1(s)P_1(s)Q_1(s) + \beta e^{j\theta}F_1(s)P_2(s)Q_2(s)$$

$$= F_1(s)P_1(s)Q_1(s) + \left[1+\beta e^{j\theta}\frac{F_1(s)}{F_2(s)}\right]F_2(s)P_2(s)Q_2(s)$$

is Hurwitz for all $\theta \in [0, 2\pi)$ and $\mathbf{p} \in \mathbf{\Pi}$. Thus, the vertex polynomials can be written down as:

$$V_i(s,\beta,\theta) = V_i^N(s) + \left[1+\beta e^{j\theta}F(s)\right]V_i^D(s), \quad i = 1, 2, \cdots, 16.$$

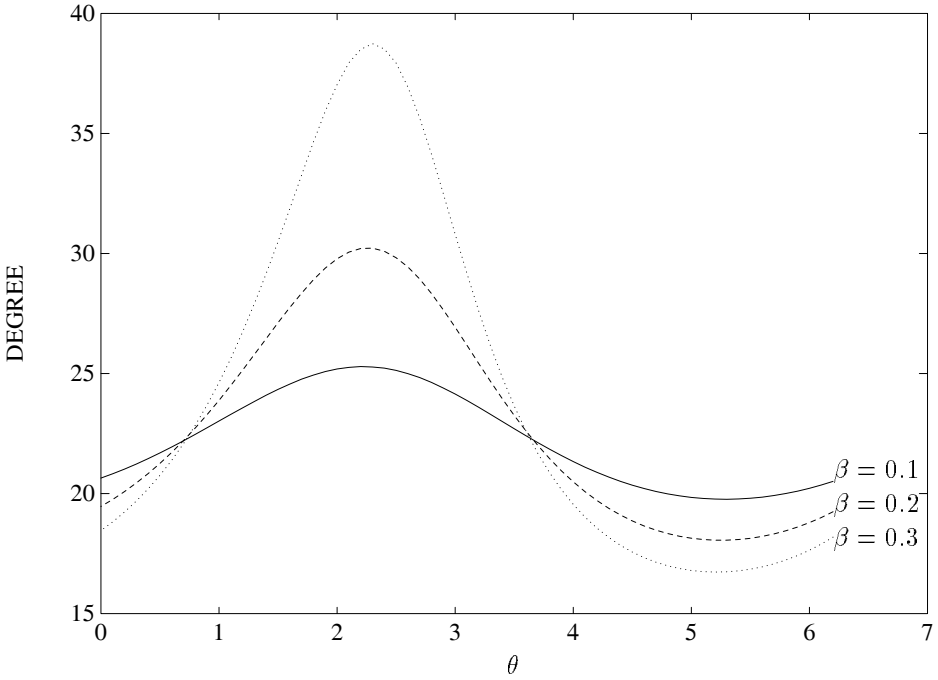

Figure 10.17. $\sup_\omega \Phi_{\mathbf{\Delta}_V}(\omega,\beta,\theta)$ vs. θ for $\beta = 0.1, 0.2, 0.3$. (Example 10.5(d))

A lower bound $\underline{\beta}$ on the worst case H_∞ stability margin β^* is obtained by selecting the largest positive value of β such that the Bounded Phase Condition

is satisfied for all $\theta \in [0, 2\pi)$. Equivalently,

$$\underline{\beta} = \inf_{\beta \geq 0} \left\{ \beta \ : \ \sup_{\theta} \sup_{\omega} \Phi_{\mathbf{\Delta}_{\mathrm{v}}}(\omega, \beta, \theta) = 180^{\circ} \right\}.$$

Figure 10.17 shows the maximum phase difference over the vertices and over all frequency for every fixed β. From Figure 10.18 we find that for any $\beta < 0.49$,

$$F_1(s)P_1(s)Q_1(s) + \left[1 + \beta e^{j\theta} \frac{F_1(s)}{F_2(s)}\right] F_2(s)P_2(s)Q_2(s)$$

is Hurwitz for all $\theta \in [0, 2\pi)$.

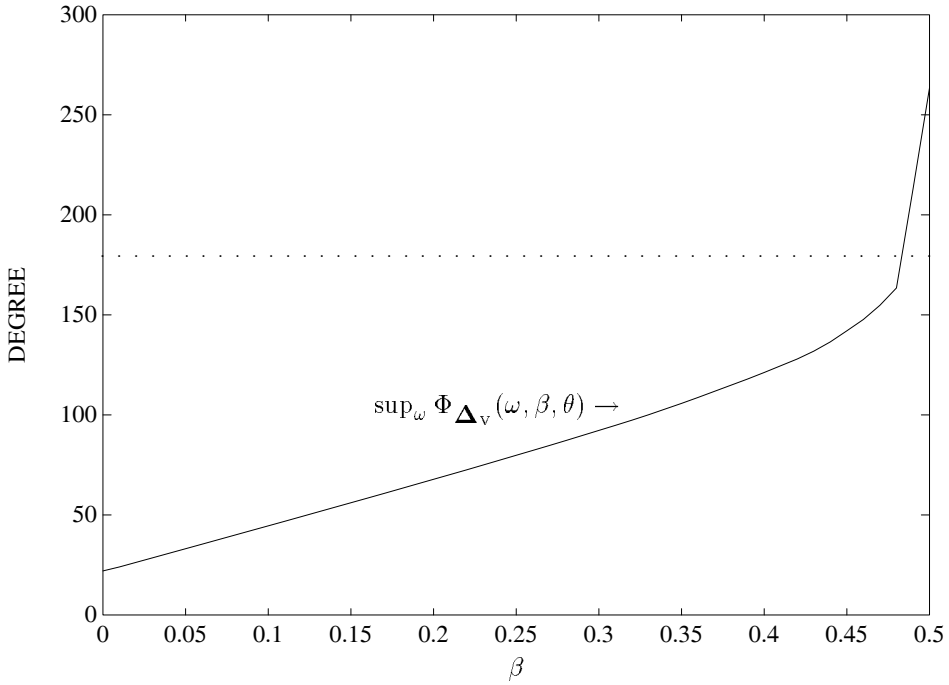

Figure 10.18. $\sup_{\omega} \Phi_{\mathbf{\Delta}_{\mathrm{v}}}(\omega, \beta, \theta)$ vs. β.(Example 10.5(d))

Thus, the lower bound on the worst case H_∞ stability margin is

$$\underline{\beta} \approx 0.49.$$

Now we can find an upper bound $\bar{\beta}$ by determining the H_∞ stability margins of the vertices and it turns out to be $\bar{\beta} \approx 0.49$. From these bounds we see that

$$\beta^* \approx 0.49.$$

Remark 10.1. Similar calculations can be used to estimate the size of the sector containing nonlinear gains for which a multilinear interval system remains absolutely stable. In other words, once we replace the multilinear family by the polytopic family $\bar{\mathbf{M}}(s)$, we may use the Lur'e, Popov or Circle Criterion to determine lower bounds on the size of the Robust Absolute Stability Sector. From the vertex systems we can find an upper bound on this sector. Exercise 10.1 deals with this type of problem.

Remark 10.2. Our definition of the multilinear interval system $\mathbf{M}(s)$ assumes that the numerator and denominator parameters $\mathbf{q}$ and $\mathbf{r}$ are independent. This restriction can be relaxed by replacing $M(s)$ by a linear fractional transformation $F(M(s))$ for all $M(s) \in \mathbf{M}(s)$. We simply construct the polytopic family $\bar{\mathbf{M}}(s)$ and replace the set $F(\mathbf{M}(s))$ by the set $F(\bar{\mathbf{M}}(s))$. From the image set bounding property of $\bar{\mathbf{M}}(s)$ and the fact that linear fractional transformations preserve boundaries it follows that at every point $s^* \in \mathbb{C}$:

$$F(\mathbf{M}(s^*)) \subset F(\bar{\mathbf{M}}(s^*)).$$

It is easy to see from the above that all the results and calculations derived in this chapter carry over to the set $F(\mathbf{M}(s))$. Since linear fractional transformations are a large class of transformations, this allows us to handle all sorts of dependencies in a convenient way. This is explored in Exercise 10.2.

10.6 EXERCISES

10.1 For the system given in Example 10.5, estimate the size of the sector containing nonlinear gains for which the entire multilinear family of closed loop systems remains robustly absolutely stable. Estimate the sectors using respectively the

a) Lur'e criterion

b) Popov criterion

c) Circle criterion.

10.2 In the feedback system shown below in Figure 10.19.
Let

$$G(s) = \frac{s+\alpha}{s+\beta}, \qquad C_1(s) = \frac{s+2}{s+3}, \qquad C_3(s) = \frac{2}{s+4}$$

with the nominal values $\alpha^0 = 1$, $\beta^0 = -5$.

a) Find a controller $C_2(s)$ that stabilizes the nominal closed loop system.

b) With the controller obtained in a), let $\alpha \in [1-\epsilon, 1+\epsilon]$ and $\beta \in [-5-\epsilon. -5+\epsilon]$. Find the maximum value of ϵ for which the closed loop system remains robustly stable.

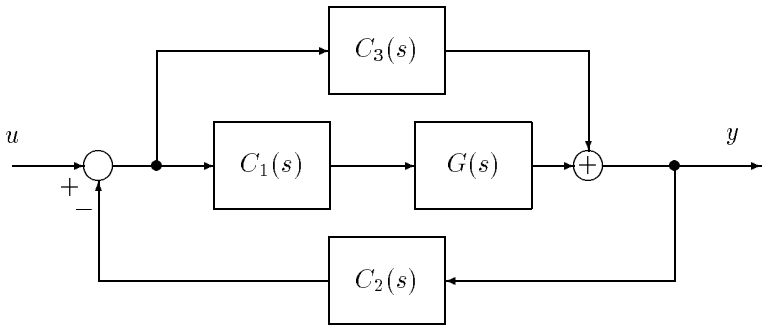

Figure 10.19. Feedback system (Exercise 10.2)

10.3 Consider the feedback system shown in Figure 10.20.

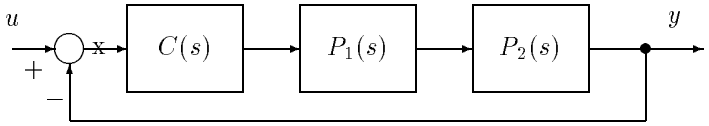

Figure 10.20. Feedback system (Exercise 10.3)

Let

$$C(s) = \frac{1}{s+1}, \quad P_1(s) = \frac{p_0}{s+q_0}, \quad P_2(s) = \frac{p_1}{s+q_1}$$

and let the parameters range over

$$q_0 \in [0.5, 1.5], \quad p_0 \in [0.5, 1.5], \quad q_1 \in [1.5, 2.5], \quad p_1 \in [0.5, 1.5].$$

a) Verify that the closed loop system is robustly stable.

b) Construct the polytopic system $\bar{\mathbf{M}}(s)$.

c) Using the polytopic system $\bar{\mathbf{M}}(s)$, estimate the maximum guaranteed gain margin measured at the loop breaking point "x".

d) Likewise estimate the maximum guaranteed phase margin at "x".

10.4 In the the feedback system of Exercise 10.3, suppose we want to expand the range of allowable parameter variations by letting the parameters vary as

$$q_0 \in [0.5 - \epsilon, 1.5 + \epsilon], \quad p_0 \in [0.5 - \epsilon, 1.5 + \epsilon],$$

$$q_1 \in [1.5 - \epsilon, 2.5 + \epsilon], \quad p_1 \in [0.5 - \epsilon, 1.5 + \epsilon].$$

What is the maximum value of ϵ for which the polytopic system $\bar{\mathbf{M}}(s)$ does not lose robust stability?

10.5 Suppose that unstructured additive uncertainty is introduced into the system in Exercise 10.3 as shown in Figure 10.21:

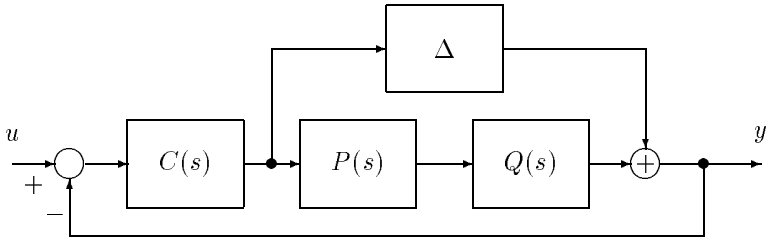

Figure 10.21. Feedback system with additive H_∞ uncertainty (Exercise 10.5)

Estimate the maximum additive H_∞ uncertainty that the closed loop system can tolerate, by using the polytopic system $\bar{\mathbf{M}}(s)$.

10.6 Suppose that unstructured perturbation is applied to the system in Exercise 10.3 in a multiplicative form as shown below in Figure 10.22.

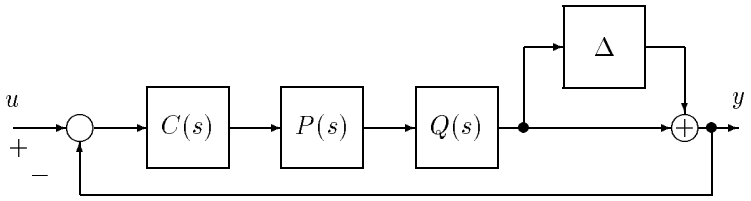

Figure 10.22. Feedback system with multiplicative H_∞ uncertainty (Exercise 10.6)

Find the maximum multiplicative H_∞ stability margin possessed by the closed loop system.

10.7 Suppose that a time-delay block, e^{-sT} is inserted at "x" in the feedback system of Exercise 10.3 (see Figure 10.20). Find a lower bound in the the time-delay that can be robustly tolerated by the closed loop system, using the polytopic system $\bar{\mathbf{M}}(s)$.

10.8 Consider the feedback system shown below in Figure 10.23.

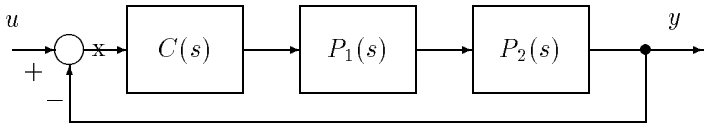

Figure 10.23. Feedback system (Exercise 10.8)

Let

$$C(s) = \frac{1}{s+1}, \qquad P_1(s) = \frac{s+\beta_0}{\alpha_1 s + \alpha_0}, \qquad P_2(s) = \frac{s+\delta_0}{\gamma_1 s + \gamma_0}.$$

and

$$\begin{aligned} &\alpha_1 \in [1,2], \quad \beta_0 \in [1,2], \quad \gamma_1 \in [1,5] \\ &\alpha_0 \in [1,2], \quad \delta_0 \in [1,3], \quad \gamma_0 \in [6,10]. \end{aligned}$$

a) Verify that the closed loop system is robustly stable.

b) Construct the polytopic system $\bar{\mathbf{M}}(s)$.

c) Using the polytopic system $\bar{\mathbf{M}}(s)$, find the maximum guaranteed gain margin measured at the loop breaking point "x".

d) Similarly estimate the maximum guaranteed phase margin measured at the point "x".

10.9 In the the feedback system of Exercise 10.8, suppose we want to expand the range of allowable parameter variations by letting the parameters vary as

$$\alpha_1 \in [1-\epsilon, 2+\epsilon], \quad \beta_0 \in [1-\epsilon, 2+\epsilon], \quad \gamma_1 \in [1-\epsilon, 5+\epsilon],$$

$$\alpha_0 \in [1-\epsilon, 2+\epsilon], \quad \delta_0 \in [1-\epsilon, 3+\epsilon], \quad \gamma_0 \in [6-\epsilon, 10+\epsilon].$$

Calculate the maximum value of ϵ for which the polytopic system $\bar{\mathbf{M}}(s)$ remains robustly stable?

10.10 Consider the feedback system shown below (Figure 10.24):
Let

$$C(s) = 2, \qquad P_1(s) = \frac{s+\beta_0}{s^2 + \alpha_1 s + \alpha_0}, \qquad P_2(s) = -\frac{s+\delta_0}{s+\gamma_0}$$

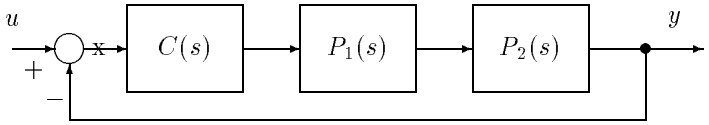

Figure 10.24. Feedback system (Exercise 10.10)

with

$$\alpha_1 \in [3,6], \quad \alpha_0 \in [1,2], \quad \delta_0 \in [1,2]$$
$$\gamma_0 \in [4,6], \quad \beta_0 \in [3,5].$$

a) Check whether the closed loop system is robustly stable.

b) Construct the polytopic system $\bar{\mathbf{M}}(s)$.

c) Using the polytopic system $\bar{\mathbf{M}}(s)$, estimate the maximum guaranteed gain margin at the loop breaking point "x".

d) Estimate the maximum guaranteed phase margin at "x".

10.11 In the the feedback system of Exercise 10.10, suppose we want to expand the range of allowable parameter variations by letting the parameters vary as

$$\alpha_1 \in [3-\epsilon, 6+\epsilon], \quad \alpha_0 \in [1-\epsilon, 2+\epsilon], \quad \delta_0 \in [1-\epsilon, 2+\epsilon],$$
$$\gamma_0 \in [4-\epsilon, 6+\epsilon], \quad \beta_0 \in [3-\epsilon, 5+\epsilon].$$

Evaluate the maximum value of ϵ for which the polytopic system $\bar{\mathbf{M}}(s)$ remains robustly stable?

10.7 NOTES AND REFERENCES

The Mapping Theorem was stated and proved in the 1963 book of Zadeh and Desoer [243]. It was effectively used in parametric stability margin calculations by deGaston and Safonov [80] and Sideris and Sanchez-Pena [210]. The mixed uncertainty stability margin calculations given in Section 10.3 were developed by Keel and Bhattacharyya [133, 134].

Vicino, Tesi and Milanese [230] gave an algorithm for calculating parametric stability margins in the case of nonlinearly correlated parameter dependence. In Hollot and Xu [118], Polyak [190] and Anderson, Kraus, Mansour and Dasgupta [10] conditions under which the image set of a multilinear interval polynomial reduces to a polygon are investigated.